

# Science



1  
2  
3  
4  
5  
6  
7  
8  
9  
10  
11  
12  
13  
14  
15  
16  
17  
18  
19  
20  
21  
22  
23  
24  
25  
26  
27  
28  
29

## Supplementary Materials for

### **Neuropilin-1 is a host factor for SARS-CoV-2 infection**

James L. Daly, Boris Simonetti\*, Katja Klein, Kai-En Chen, Maia Kavanagh Williamson, Carlos Antón-Plágaro, Deborah K. Shoemark, Lorena Simón-Gracia, Michael Bauer, Reka Hollandi, Urs F. Greber, Peter Horvath, Richard B. Sessions, Ari Helenius, Julian A. Hiscox, Tambat Teesalu, David A. Matthews, Andrew D. Davidson, Brett M. Collins, Peter J. Cullen\*, Yohei Yamauchi\*.

\* Corresponding Authors. Email:

[bs13866@bristol.ac.uk](mailto:bs13866@bristol.ac.uk)

[pete.cullen@bristol.ac.uk](mailto:pete.cullen@bristol.ac.uk)

[yohei.yamauchi@bristol.ac.uk](mailto:yohei.yamauchi@bristol.ac.uk)

### **This PDF file includes:**

Materials and Methods  
Figs. S1 to S5  
Tables S1 to S3

## 30 **Materials and Methods**

### 31 **Antibodies and reagents**

32 The following antibodies were used in this study: mouse anti- $\beta$  actin (Sigma-Aldrich, A1978, WB  
33 1:2000), mouse anti-ACE2 (Proteintech, 66699-1-Ig, WB 1:1000), mouse anti-GFP (Roche,  
34 11814460001, WB 1:2000), rabbit anti-mCherry (Abcam, ab167453, WB 1:2000), rabbit anti-  
35 NRP1 (Abcam, ab81321, WB 1:1000), rabbit anti-SARS-CoV-2 Spike RBD (S1 epitope) (Sino  
36 Biologicals, 40592-T62, WB 1:1000), rabbit anti-SARS nucleocapsid (N) polyclonal antibody  
37 (ROCKLAND, 200-401-A50, IFA 1:2000), mouse anti-SARS-CoV-2 Spike antibody [1A9] (S2  
38 epitope) (GeneTex, GTX632604, WB 1:1000). Recombinant human ACE2 was purchased from  
39 Sino Biological (10108-H08H). EG 00229 trifluoroacetate was purchased from Tocris (6986). The  
40 monoclonal antibody against the hemagglutinin of influenza A/duck/New  
41 Zealand/164/76(H11N3) was a kind gift of Robert Webster.

42

### 43 **Cell culture and transfection**

44 Calu-3, Caco-2 (a kind gift from Dr Darryl Hill), Caco-2 shSCR and shNRP1 (a kind gift from  
45 Giuseppe Balistreri), HeLa, HEK293T and Vero E6 cell lines were originally sourced from the  
46 American Type Culture Collection. Authentication was from the American Type Culture  
47 Collection. We did not independently authenticate the cell lines. Cells were grown in DMEM  
48 medium (Sigma-Aldrich) supplemented with 10% (vol/vol) FCS (Sigma-Aldrich) and  
49 penicillin/streptomycin (Gibco) with the exception of Calu-3 cells that were grown in Eagle's  
50 minimal essential medium (MEM+GlutaMAX; Gibco™, ThermoFischer) supplemented with 10%  
51 FCS 0.1mM non-essential amino acids (NEAA), 1mM sodium pyruvate, 100 IU/ml streptomycin  
52 and 100  $\mu$ g/ml penicillin. Caco-2 cells were maintained in DMEM+GlutaMAX, 10% FCS and

53 0.1mM NEAA. FuGENE HD (Promega) was used for transient transfection of DNA constructs  
54 for infection assays according to the manufacturer's instructions. PPC-1 human primary prostate  
55 cancer cells were obtained from Erkki Ruoslahti laboratory at Cancer Research Center, Sanford-  
56 Burnham-Prebys Medical Discovery Institute. M21 human melanoma cells were obtained from  
57 David Cheresch at University of California San Diego. Cos-7 cells were obtained from Urs Greber  
58 laboratory. Cells were cultured in DMEM medium containing 100 IU/mL of streptomycin,  
59 penicillin, and 10% FBS in 37°C incubator with 5% CO<sub>2</sub>.

60

61 To generate a NRP1-null HeLa cell line, the following guide RNA (gRNA) was cloned into  
62 pSpCas9(BB)-2A-Puro (PX459): 5'-GATCGACGTTAGCTCCAACG-3'. gRNA was transfected  
63 into HeLa cells using FuGENE HD. 24 hours later, transfected cells were selected with puromycin.  
64 Selected cells were trypsinised and diluted to a concentration of 2.5 cells mL<sup>-1</sup> in Iscove's modified  
65 Dulbecco's medium (Gibco) supplemented with 10% (vol/vol) FBS (Sigma-Aldrich). 200 µL of  
66 this suspension was plated into 96-well plates to seed single cell colonies. After three weeks,  
67 colonies were expanded and lysed, and knockout was validated by immunoblotting for NRP1.

68

### 69 **Generation of stable lentiviral cell lines**

70 The genes of interest were subcloned into the lentiviral vector pLVX for the generation of lentiviral  
71 particles. Lentiviral particles were produced and harvested in HEK293T cells. HeLa cells were  
72 transduced with lentiviral particles to produce stably expressing cell lines. Following transduction,  
73 pLVX-expressing cells were selected with puromycin or blasticidin accordingly.

74

75

76 **SARS-CoV-2 isolation and infection**

77 A clinical specimen in viral transport medium, confirmed SARS-CoV-2 positive by qRT-PCR  
78 (kindly proved by Dr Lance Turtle, University of Liverpool), was adjusted to 2 ml with OptiMEM  
79 (Gibco™, ThermoFisher), filtered through a 0.2 µm filter and used to infect Vero E6 cells. After  
80 1 h the inoculum was diluted 1:3 (vol/vol) with MEM supplemented with 2% FCS and incubated  
81 at 37 °C in a 5% CO<sub>2</sub> incubator for 5 days. The culture supernatant was passaged twice more on  
82 Vero E6 cells until cytopathic effect was observed and then once on Caco-2 cells to produce the  
83 stock used in the experiments. The intracellular viral genome sequence and the titre of virus in the  
84 supernatant were determined as previously described (20) and the virus termed SARS-CoV-  
85 2/human/Liverpool/REMRQ0001/2020. A stock of the SARS-CoV-2 strain SARS-CoV-2 strain  
86 England/2/2020 (VE6-T) containing a mixture of the wild type virus and a virus in which  
87 the RRAR furin cleavage site had been deleted (SARS-CoV-2 ΔS1/S2) (20) was serially diluted  
88 (10-fold dilutions) in MEM supplemented with 2% FCS and added to either Vero E6 or Caco-2  
89 cells in a 96 well plate. After 5 days incubation at 37 °C in 5% CO<sub>2</sub>, the culture supernatants in  
90 wells showing CPE at the highest dilution were again diluted and passaged on the same cells. After  
91 a further 5 days incubation, a 20 µl aliquot of culture supernatant from wells showing CPE at the  
92 highest dilution were used for RNA extraction and RT-PCR using a primer set designed to  
93 discriminate the wild type and SARS-CoV-2 ΔS1/S2 viruses. Culture supernatants containing  
94 either the wild type virus or the SARS-CoV-2 ΔS1/S2 virus, with no sign of a mixed virus  
95 population were used to produce large scale stocks in Vero E6 cells. The presence of the expected  
96 virus in the stocks was verified by direct RNA sequencing using an Oxford Nanopore flow cell as  
97 previously described (18). For virus infections, virus was added directly to culture medium of the  
98 target cells in a 96-well plate at the required infectious dose and the plates incubated at 37 °C for

99 16 h. The culture supernatant was removed, and the cells fixed with 4% (vol/vol)  
100 paraformaldehyde (PFA) for 1 h at room temperature. All work with infectious SARS-CoV-2 was  
101 done inside a class III microbiological safety cabinet in a containment level 3 facility at the  
102 University of Bristol.

103

#### 104 **Pseudotyped virus generation**

105 The VSV $\Delta$ G system was a kind gift from Stefan Pöhlmann, and used to generate pseudovirus  
106 particles decorated with SARS-2-S or VSV-G as described previously (5, 21) with some  
107 modifications. Briefly, HEK293T cells were grown in 100 mm diameter dishes to 90% confluency  
108 and were subsequently transfected with 6  $\mu$ g of pCG1\_SARS-2-S or pCMV-VSV-G plasmid using  
109 polyethylenimine (PEI) Max (MW = 40,000KDa, Polysciences, Germany) as transfection reagent.  
110 Transfection was performed using a PEI:DNA ratio of 4:1 in serum free DMEM for 4 hours at  
111 37°C. The cells were then washed with PBS and cultured in fresh complete DMEM supplemented  
112 with 5% FBS at 37°C overnight. The next day cells were exposed to the replication deficient  
113 VSV\* $\Delta$ G-fLuc vector (kindly provided by Markus Hoffmann, German Primate Center, Leibnitz)  
114 for 2 hours at 37°C. The cells were then washed with PBS before the addition of medium  
115 supplemented with anti-VSV-G I1 antibody (kindly provided by Markus Hoffmann, German  
116 Primate Center, Leibnitz). No I1 antibody was added to VSV-G expressing cells. The cells were  
117 further incubated at 37°C for 24 hours before the supernatant was harvested and clarified by  
118 centrifugation at 2,000 x g for 10 minutes. For immunoprecipitation experiments, VSV pseudoviral  
119 particles were concentrated 10-fold using 100KDa Amicon<sup>®</sup> Ultra centrifugal filter units.

120

#### 121 **Infection assays, indirect immunofluorescence, automated confocal imaging**

122 For infection assays, cells seeded in Clear 96-well Microplates (Greiner Bio-one) were infected  
123 with SARS-CoV-2/human/Liverpool/REMRQ001/2020 isolate in MEM, 2% FCS, supplemented  
124 with 0.1mM NEAA and fixed in 4% PFA in PBS at 16 h.p.i. After permeabilisation with 0.1%  
125 TritonX-100 in PBS, 1% BSA, the cells were blocked and stained in 1% BSA in PBS containing  
126 anti-SARS Nucleocapsid (N) rabbit polyclonal antibody or anti-SARS Spike (S) monoclonal  
127 antibody and further stained with Hoechst (1:10000) and appropriate Alexa Fluor (488/594/647)-  
128 conjugated secondary antibodies (Thermo Fisher Scientific). The stained plates were imaged using  
129 an automated high-content spinning-disk microscope CQ1 (Confocal Quantitative Image  
130 Cytometer, Yokogawa, Japan) using UPlanSApo 10x/0.4na, UPlanSApo 20x/0.75na or  
131 UPlanSApo 40x/0.95na objectives (Olympus, Japan). To capture a single 96-well, 20 fields (with  
132 10x objective) or 80 fields (20x) were imaged by z-stacks at 5 µm intervals and maximum intensity  
133 projected for analysis. Yokogawa CQ1 imaging was performed with four excitation laser lines  
134 (405/488/561/640nms) with spinning disc confocal.

135

### 136 **Virus binding and uptake assay**

137 SARS-CoV-2 wt was inoculated at an MOI=50 on Caco-2 cells grown in Clear 96-well  
138 Microplates (Greiner Bio-one) and allowed to bind to the cell surface in the cold on a chilled metal  
139 plate for 60 min. For the binding assay, cells were fixed immediately after. For the virus uptake  
140 assay, the inoculum was removed after binding and incubated for 30 min on a pre-warmed metal  
141 block at 37 °C in the presence of 1 mM cycloheximide, and fixed. To distinguish extracellular and  
142 intracellular viral particles, a two-step, dual staining procedure was used using antibodies against  
143 SARS-CoV-2 S and N, in that order. Briefly, the fixed cells were blocked in PBS, 1% BSA for 30  
144 min followed by staining with anti-S (1:250) for 60 min at room temperature, washed and stained

145 with goat anti-rabbit Alexa Fluor 488 (1:2500) and wheat germ agglutinin conjugated with Alexa  
146 Fluor 647 (1:250) for 30 min, washed and fixed for 15 min in 4% FA in PBS. The cells were then  
147 permeabilized for 2 min in PBS, 1% BSA, 0.1% Tx-100, washed and stained with anti-N (1:2000)  
148 for 60 min at room temperature, then washed and stained with goat anti-rabbit Alexa Fluor 594 for  
149 30 min to stain all extracellular and intracellular viral particles. Hoechst was used to stain nuclei.  
150 Where indicated phalloidin conjugated to Alexa Fluor 647 (1:250) was used to image actin  
151 filaments. The cells were imaged using the Yokogawa CQ1 automated spinning-disk microscope  
152 with a UPlanSApo 40x/0.95na objective (Olympus, Japan), acquiring 20 z-stacks at 0.6  $\mu\text{m}$   
153 intervals using 4 channels. Nine to 16 fields of view were captured via well and the resulting MIP  
154 images were used for image analysis using the Cell Path Finder software (Yokogawa).

155

#### 156 **Cell immunostaining and confocal microscopy**

157 PPC-1, M21 and HeLa cells were seeded in a 24-well plate (50,000 cells/well) with coverslips and  
158 allowed to grow until the next day. The medium was removed, the cells were washed twice with  
159 PBS pH 7.4, and fixed with 4% PFA in PBS for 10 min at room temperature. The cells were  
160 washed twice with PBS and once with PBST (PBS with 0.05 % Tween-20). Blocking buffer (5%  
161 BSA, 5% FBS, 5% goat serum in PBST) was added to the cells and incubated for 1 h at room  
162 temperature. The blocking buffer was removed, and 0.3 mL of monoclonal antibodies were added  
163 to the cells (mAB diluted 1 in 5 in diluted blocking buffer containing 1% BSA, 1% FBS, 1% goat  
164 serum in PBST). Cells were incubated for 1 h at room temperature and washed 3 times with PBST.  
165 Secondary antibody AlexaFluor 546 goat anti-mouse IgG (Invitrogen Molecular Probes, Cat. No.  
166 A11003) was added to the cells (4 $\mu\text{g}/\text{mL}$  in diluted blocking buffer). Cells were incubated for 30  
167 min at room temperature, washed 3 times with PBS and stained with 1 $\mu\text{g}/\text{mL}$  of DAPI for 10 min

168 at room temperature. After three washes with PBS, the cells were mounted on glass slides with  
169 mounting media (Fluoromount-G; Electron Microscopy Sciences) and sealed with nail polish. A  
170 confocal microscope FV1200MPE (Olympus, Japan) was used for cell imaging of PPC-1 and M21  
171 cells with an UPlanSApo 60x/1.35na objective (Olympus, Japan). The images were analyzed using  
172 Olympus FluoView Ver.4.2a Viewer software. HeLa cells were imaged with a confocal laser  
173 scanning microscope (SP5II AOBS, Leica Microsystems) attached to an inverted epifluorescence  
174 microscope (DMI600, Thermo Fischer Scientific) with a 40X/1.25na objective. Fluorescence  
175 intensity of surface NRP1 was quantified using Volocity software.

176

### 177 **Image analysis**

178 Projected images taken with a 20x objective were used for image analysis for single-cell and  
179 multinucleated cell infection image analysis with supervised machine learning. Image processing  
180 was performed using the BIAS software (Single-Cell Technologies Inc., Hungary). Firstly, images  
181 of each fluorescence channel were corrected using the CIDRE illumination correction method (22).  
182 Individual cell nuclei were detected by a deep machine learning-based segmentation algorithm  
183 NucleAIzer (11). Cellular cytoplasm were detected both on the green and red channels using  
184 UNET to enhance fluorescence images (23). The method was trained to precisely delineate often  
185 faint signals in the cytoplasm. Cellular phenotypes were assigned to each individual nucleus. These  
186 are infected cells which contain a single nucleus (Single Cell Infection), those that contain more  
187 multiple nuclei (Multi Nuclei Infection) as observed in the distinct cell-cell fusion syncytia  
188 phenotype. Supervised machine learning was used for phenotypic assignment. The decisions were  
189 based on single-cell and its microenvironment's morphology and intensity features (24). Final



190 statistics include the number of multi-nucleated cells, the average number of nuclei in these cells  
191 and the count of other phenotypic classes. Yokogawa CQ1 was also used for image quantification.

192

### 193 **Immunoprecipitation and quantitative western blot analysis**

194 Cells were lysed in PBS with 1% Triton X-100 and protease inhibitor cocktail for western blotting.

195 The protein concentration was determined using a BCA assay kit (Thermo Fisher Scientific) and

196 equal amounts were resolved on NuPAGE 4–12% precast gels (Invitrogen). Blotting was

197 performed onto polyvinylidene fluoride membranes (Immobilon-FL, EMD Millipore), followed

198 by detection using the Odyssey infrared scanning system (LI-COR Biosciences). When using the

199 Odyssey, we routinely performed western blot analysis where a single blot was simultaneously

200 probed with antibodies against two proteins of interest (distinct antibody species), followed by

201 visualization with the corresponding secondary antibodies conjugated to distinct spectral dyes. The

202 band intensities, normalized to actin expression, are presented as the average fraction of protein

203 abundance relative to control conditions.

204

205 For the GFP- and mCherry-based immunoprecipitations, HEK293T cells were transfected with

206 GFP or mCherry constructs using PEI (Sigma-Aldrich). The cells were lysed in

207 immunoprecipitation buffer (50mM Tris–HCl, 0.5% NP-40 PBS with protease inhibitor cocktail

208 (Roche)) 24hr after transfection and subjected to GFP-trap (ChromoTek) or RFP-tap (ChromoTek)

209 beads. To inhibit immunoprecipitation of GFP-S1 constructs, EG00229 or mAb#3 were added to

210 the immunoprecipitation buffer at the indicated concentrations, DMSO and PBS were respectively

211 used as controls. Following immunoprecipitation, the beads were washed twice in 50mM Tris-

212 HCl, 0.25% NP40 PBS with protease inhibitor cocktail, pH 7.5, and once in 50mM Tris-HCl PBS

213 with protease inhibitor cocktail, pH 7.5, before boiling in 2X LDS sample loading buffer for  
214 elution. Immunoblotting was performed using standard procedures. Detection was performed on  
215 an Odyssey infrared scanning system (LI-COR Biosciences) using fluorescently labelled  
216 secondary antibodies. Band intensities are normalized to the amount of immunoprecipitated  
217 protein levels (of GFP-tagged constructs for GFP-nanotrap experiments, and of mCherry-tagged  
218 constructs for mCherry-nanotrap experiments). The band intensities are then presented as the  
219 average fraction of immunoprecipitated protein abundance relative to the amount  
220 immunoprecipitated in control conditions.

221

222 For immunoprecipitation of the VSV-Spike pseudotyped virus, mCherry, mCherry-b1 and  
223 mCherry-b1 T316R were transfected into HEK293T cells the day before immunoprecipitation.  
224 Cells were lysed in 50mM Tris-HCl 0.5% NP40 PBS with protease inhibitor cocktail, pH 7.5.  
225 Lysates were cleared by centrifugation at 20,000 g for 10 minutes at 4°C. From the resulting  
226 supernatant, an input fraction was reserved, and the rest incubated with RFP-trap beads to rotate  
227 for 1 hour at 4°C. Following enrichment of mCherry constructs, the beads were washed twice in  
228 50mM Tris-HCl 0.25% NP40 PBS with protease inhibitor cocktail, pH 7.5, and twice in 50mM  
229 Tris-HCl PBS with protease inhibitor cocktail, pH 7.5, to remove residual cell lysate and detergent.  
230 VSV-Spike pseudotyped virus was added to the isolated mCherry beads and incubated rotating for  
231 a further 1 hour at 4°C. Following virus immunoprecipitation, the beads were again washed twice  
232 in 50mM Tris-HCl 0.25% NP40 PBS with protease inhibitor cocktail, pH 7.5, and twice in 50mM  
233 Tris-HCl PBS with protease inhibitor cocktail, pH 7.5, before boiling in 2X LDS sample loading  
234 buffer for elution.

235

236 **Recombinant NRP1 b1 and b1b2 soluble protein expression and purification**

237 The sequence encoding the human NRP1 b1 domain composed of residues 273-427 was  
238 synthesized and sub-cloned into the pET28a(+) at NdeI and XhoI restriction sites, for bacterial  
239 expression with an N-terminal His-tag. The protein was expressed in Rosetta-gami<sup>TM</sup> 2 (DE3) cells  
240 (Novagen) similar to the protocol described previously (25, 26). In brief, the protein was expressed  
241 in Terrific-Broth at 37°C until OD<sub>600</sub> reached 1.5. The culture was then cooled 15 min at 4°C prior  
242 to induction with 1 mM isopropyl β-D-thiogalactopyranoside (IPTG). The culture was further  
243 expressed for ~16 h at 16°C before harvesting. Cell pellets were lysed using a constant system TS-  
244 series cell disruptor in lysis buffer containing 50 mM Tris-HCl (pH 7.5), 300 mM NaCl, 50 μg/ml  
245 benzamidine and DNase I. The homogenate was cleared by centrifugation and loaded onto Talon®  
246 resin (Clontech) using standard affinity purification procedures. Removal of the His-tag was  
247 performed by adding thrombin (Sigma-Aldrich) into the eluted fraction together with dialysis  
248 overnight in the lysis buffer at 4°C. The cleaved and uncleaved fractions were then separated using  
249 reverse metal affinity chromatography. The His-tag cleaved fraction was collected and further  
250 purified by gel filtration using Superdex 75 16/60 column in either neutral pH buffer containing  
251 50 mM Tris-HCl pH 7.5, 150 mM NaCl or acidic buffer containing 50 mM sodium citrate pH 5.5,  
252 150 mM NaCl.

253  
254 Wild-type and triple mutant human NRP1 b1b2 domain (residues 274-584) were expressed  
255 in *Escherichia coli* strain Rosetta-gami-2 (Novagen, Madison, WI) as a His-tag fusion in pET28b  
256 (Novagen). Cells were grown in Terrific-Broth at 37°C to an OD<sub>600</sub> = 1.2 and, after 15 min at  
257 4°C, induced with 1 mM IPTG. After growth at 16°C for 16 h, cells were harvested by  
258 centrifugation, lysed, and centrifuged, and proteins were purified over HIS-Select (Sigma–Aldrich,

259 St. Louis, MO) nickel affinity resin in 20 mM Tris (pH 8.0) and 400 mM NaCl with an imidazole  
260 gradient from 25-500 mM. Further purification was performed on 5 ml hitrap heparin column  
261 (GE). Protein was loaded in 20mM Tris pH=8.0, 100mM NaCl and eluted using a linear gradient  
262 100-800 M NaCl. Final purification was performed using Superdex 75 16/100 (Amersham  
263 Pharmacia) column equilibrated in 20mM Tris pH 8.0, 150mM NaCl.

264

### 265 **Generation of monoclonal antibodies against NRP1 b1b2**

266 Female BALB/c and C57BL/6 mice, 8–9 weeks old, were immunized intraperitoneally with 17 µg  
267 of recombinant NRP1 b1b2 mixed with an equal volume of complete Freund's adjuvant (Sigma–  
268 Aldrich Chemie, Steinheim, Germany), followed by a booster immunization four weeks later of  
269 the same dose mixed with incomplete Freund's adjuvant (Sigma–Aldrich). Mice received three  
270 boosts of the same amount of antigen in PBS on days –3, –2, and –1 prior to fusion. Spleens were  
271 excised and the splenocytes were fused with myeloma cells (P3X63Ag8.653) according to a  
272 previously described protocol (25). Beginning on day 10 after fusion, hybridoma supernatants  
273 were screened for specific antibodies. Before experiments, the hybridoma supernatants were  
274 centrifuged at 300g for 5 min at room temperature and 500 µl dialyzed against 2 L of PBS over  
275 night at 4°C prior use.

276

277

### 278 **ELISA assay with monoclonal antibodies**

279 High affinity protein-binding 96-well plates (Nunc™ Maxisorp™ Cat No. 442404) were coated  
280 with 1 µg of protein (100 µL of 10 µg/mL of protein solution in PBS) overnight at 37°C. The wells  
281 were washed 5 times with PBS and blocked for 1 h at 37°C with blocking buffer (1% BSA,

282 0.1%Tween-20 in PBS). The mAb dilutions in blocking buffer were added to the wells and  
283 incubated for 1 h at 37°C. The wells were washed 5 times with blocking buffer and the peroxidase-  
284 conjugated affinity pure donkey anti-mouse IgG (Immuno Research Laboratories) was added  
285 (diluted 1 in 20.000 in blocking buffer). The plate was incubated for 1 h at 37°C and washed 5  
286 times with blocking buffer. The peroxidase substrate (TMB Peroxidase EIA Substrate Kit  
287 #1721067, Bio-Rad) was added as described in the manufacturer instructions. The absorbance of  
288 the samples was read at 655 nm using Tecan Sunrise microplate reader (Tecan, Switzerland).

289

## 290 **Statistical analysis**

291 Statistical analyses were performed using Prism 7 (GraphPad Software). Graphs represent means  
292 and SEM or SD, N represent biological replicates. The statistical test used for each experiment is  
293 always stated in the corresponding figure legends. For all statistical tests,  $P < 0.05$  was considered  
294 significant and is indicated by asterisks.

295

296

## 297 **Plasmids**

298 pLVX-IRES-BSD was generated by replacing the puromycin resistance cassette in pLVX-IRES-  
299 puro (Clontech) with a blasticidin resistance gene (BSD) using HiFi DNA assembly (New England  
300 Biolabs) according to the manufacturer's instructions. The primers used were 5'-  
301 TAGACGCGTCTGGAACAATC-3' and 5'-GGAAGGTCGTCTCCTTGTG-3' for the pLVX  
302 vector fragment, and 5'-ccacaaggagacgaccttcATGGCCAAGCCTTTGTCTC-3' and 5'-  
303 gattgtccagacgctctaGCCCTCCCACACATAACC-3' for the blasticidin fragment.

304

305 ACE2 was amplified by PCR using cDNA generated from human A549 cells as template. The  
306 primers used were 5'-agaactcgagaccATGTCAAGCTCTTCCTGGCTC-3' and 5'-  
307 tgtttctagaCTAAAAGGAGGTCTGAACATCATCAG-3' and carried an XhoI or an XbaI  
308 restriction site, respectively. The amplicon was digested with XhoI and XbaI and ligated into the  
309 digested pLVX-IRES-BSD vector. All plasmids were verified by Sanger sequencing.

310

311 The SARS-CoV-2 S gene was cloned into pLVX vectors using a commercially synthesized EGFP-  
312 S gene fusion plasmid (the S gene sequence was that of SARS-CoV-2 isolate Wuhan-Hu-1;  
313 GenBank: MN908947.3; GeneArt, ThermoFischer) as a template by Gibson assembly (NEB). For  
314 the untagged version, in brief, the S gene was amplified using overlapping primers and cloned into  
315 a 'pLVX-MCS-T2A-Puro' vector previously digested with EcoRI/BamHI. The isolated S1  
316 constructs and S1 truncations were amplified from commercially synthesized plasmids (GeneArt,  
317 ThermoFischer) encompassing nucleotides 20021 – 22960 and 22891 – 28830 of the SARS-CoV-  
318 2 isolate Wuhan-Hu-1 genome (GenBank: MN908947.3) and cloned in pEGFP.C1 using  
319 KpnI/BamHI. Mouse Nrp1-mCherry was a kind gift from Donatella Valdembrì. pEGFP-NRP1  
320 and pEGFP-NRP2 were kind gifts from Mu-Sheng Zeng. mCherry-tagged NRP1 and NRP2  
321 constructs were subcloned from pEGFP-NRP1 and pEGFP-NRP2.

322

### 323 **Isothermal Titration Calorimetry**

324 ITC experiments were conducted at 30°C using a Microcal ITC200 (Malvern) in buffer containing  
325 either 50 mM Tris-HCl pH 7.5, 150 mM NaCl (for neutral pH condition) or 50 mM sodium citrate  
326 pH 5.5, 150 mM NaCl (for acidic pH condition). To test the binding between NRP1 b1 and S1  
327 CendR peptide (corresponding to SARS-CoV2 residues <sup>679</sup>NSPRRAR<sup>685</sup>), both native and R685A

328 mutant forms of the peptide in the range of 700  $\mu$ M to 900  $\mu$ M were titrated into 40  $\mu$ M of NRP1  
329 b1 domain. The same protein/peptide concentrations and buffer conditions were applied to  
330 examine the interaction between NRP1 b1 and EG00229 inhibitor. The competitive effects of  
331 EG00229 on NRP1 b1 binding to the S1 CendR peptide was tested by pre-mixing 40  $\mu$ M of NRP1  
332 b1 with either 160  $\mu$ M of EG00229 or S1 CendR peptide, and then titrating with 700  $\mu$ M of either  
333 S1 CendR peptide or EG00229 in the ITC syringe respectively. In all cases, the experiments were  
334 carried out with an initial 0.4  $\mu$ l injection (not used in data processing) followed by 12 serial  
335 injections of 3.22  $\mu$ l each with 180 s intervals. The thermodynamic parameters  $K_d$ ,  $\Delta H$ ,  $\Delta G$  and -  
336  $T\Delta S$  were analyzed with Malvern software package by fitting and normalized data to a single-site  
337 binding model (**Tables S1, S2**). The stoichiometry was refined initially, and if the value was close  
338 to 1, then N was set to exactly 1.0 for calculation. All experiments were performed at least 2 to 3  
339 times to check for reproducibility of the data.

340

#### 341 **Crystallization and Data Collection**

342 All crystallization experiments were performed using hanging drop vapor diffusion under 96-well  
343 format at 20°C. For co-crystallization, 7X molar excess of native S1 CendR peptide (the same  
344 peptide used for ITC) was added to the purified NRP1 b1 in 50 mM sodium citrate pH 5.5, 150  
345 mM NaCl at a final protein concentration of 11 mg/ml. Crystals were observed in many different  
346 commercial screen conditions after 5 days, with most of the conditions containing acidic buffer  
347 with pH ranges from 5 to 6.5. The best quality crystals were obtained in a condition composed of  
348 0.1 M sodium citrate pH 5, 20% PEG 6000. Prior to the data collection, crystals were soaked in  
349 the cryoprotectant solution containing 0.1 M Sodium Citrate pH 5, 20% PEG 6000, 10% glycerol

350 and 8X molar excess of S1 CendR peptide. Diffraction data were collected to 2.36 Å on the MX1  
351 beamline at the Australian Synchrotron at 100 K.

352

### 353 **Structure Determination**

354 Diffraction data were indexed and integrated by AutoXDS and scaled using Aimless (26, 27). A  
355 molecular replacement solution using NRP1 b1 domain (PDB ID: 1KEX) as template was obtained  
356 by the program Phaser (30). Electron density for the S1 CendR peptide was readily observable  
357 after the molecular replacement. More specifically, electron density corresponding to the last two  
358 residues at the C-terminal tail of the CendR peptides, A684 and R685, could be interpreted in all  
359 four copies of the complex in the asymmetric unit without any refinement. In one particular copy,  
360 the electron density corresponding to the entire 7 residues of the S1 CendR peptide was visible for  
361 model building and figure display. Structure refinement was carried out using the PHENIX  
362 software suite with iterative rebuilding of the model (31). The program Coot was used for model  
363 rebuilding guided by  $F_o - F_c$  difference maps. After iterative rounds of refinement, the quality and  
364 geometry of the refined structure was evaluated using MolProbity (32). Data collection and  
365 refinement statistics are summarized in **Table S3**. Structural alignment was performed by using  
366 the DALI server and molecular graphics were generated using PyMOL (33).

367

### 368 **Data Deposition**

369 Coordinates and structure factors for the NRP1 b1 - S1 CendR peptide complex have been  
370 deposited at the Protein Data Bank (PDB) with accession code 7JJC. All the relevant raw data  
371 related to this study is available from the corresponding authors on request.

372



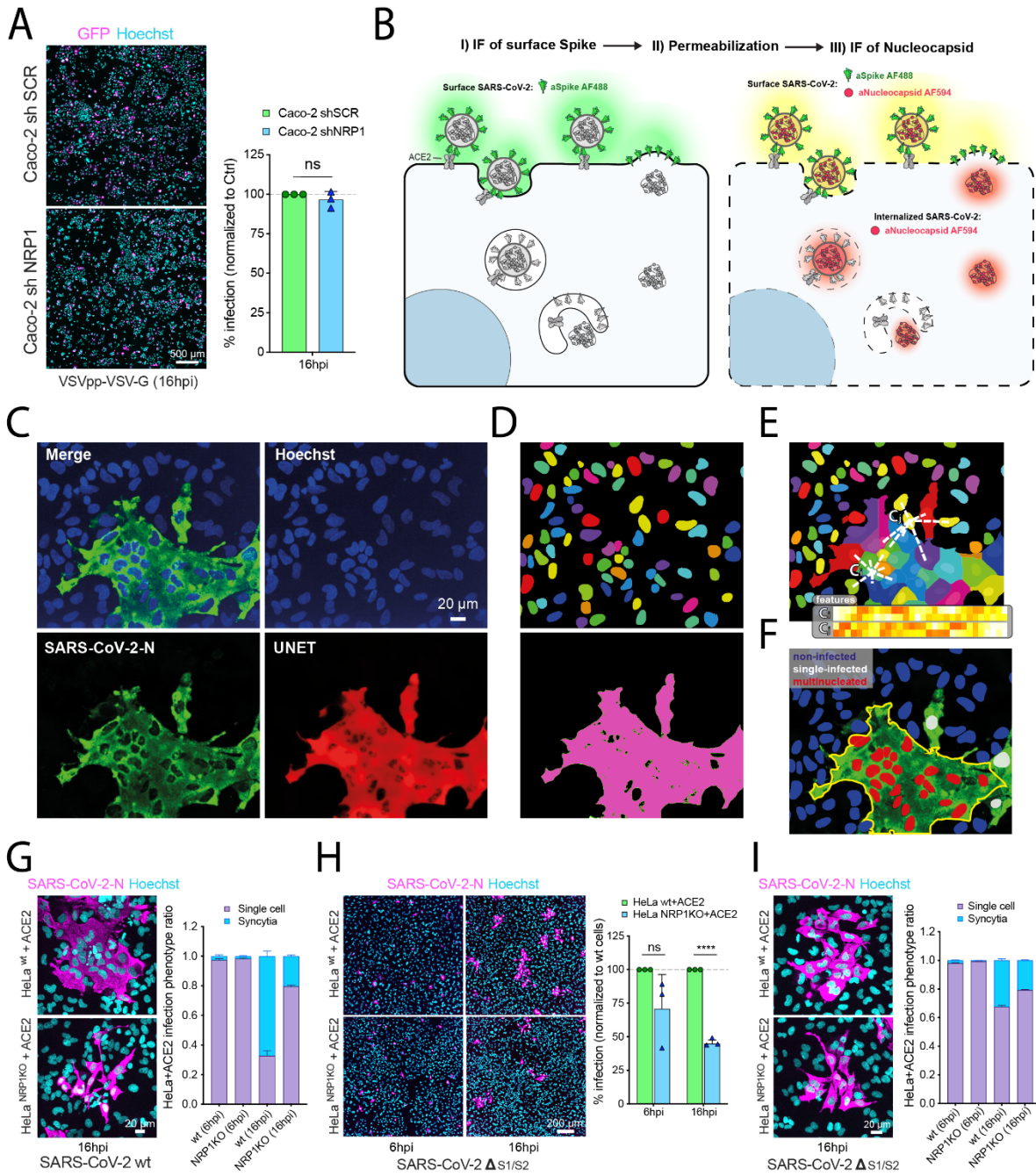


378 **Fig. S1. The SARS-CoV-2 S1 protein contains a CendR motif.** (A) Alignment of the S protein  
379 sequence of SARS-CoV and SARS-CoV-2. SARS-CoV-2 S possesses a furin cleavage site at the  
380 S1/S2 boundary that is absent in the SARS-CoV-2  $\Delta$ S1/S2 mutant. (B) Table highlighting the  
381 similarity between the C-terminal sequence of SARS-CoV-2 S1 and the CendR motifs of  
382 established NRP1 ligands. (C) Summary of constructs used in this study. TM =  
383 transmembrane. (D) SARS-CoV-2 S1 interacts with NRP2. HEK293T cells were co-transfected  
384 to express mCherry, mCherry-tagged Nrp1 or mCherry-tagged NRP2, and GFP-tagged S1, then  
385 subjected to mCherry-nanotrap (N=3). Two-tailed unpaired t-test; P= 0.2421. (E) CendR motif  
386 dependent interaction of the SARS-CoV-2 S1 with NRP2. HEK293T cells were co-transfected to  
387 express GFP-tagged S1 or GFP-S1  $\Delta$ RRAR and mCherry or mCherry-tagged NRP2, then  
388 subjected to mCherry-nanotrap. (N=4). Two-tailed unpaired t-test; P = 0.0175. (F) Quantification  
389 of ACE2 levels in HeLa<sup>wt</sup>+ACE2 and HeLa<sup>NRP1KO</sup>+ACE2 cells (N=3). Two-tailed unpaired t-test;  
390 P=0.1065. (G) HeLa<sup>wt</sup> and HeLa<sup>wt</sup>+ACE2 were infected with SARS-CoV-2, fixed 16 hpi and  
391 infection was quantified (N=3). Scale bar = 200  $\mu$ m. (H) Caco-2 cells were transfected with a  
392 control shRNA (shSCR) an anti-NRP1 shRNA (shNRP1). Following western blotting of cell  
393 lysates, NRP1 and ACE2 bands were quantified (N=3). Two-way ANOVA and Sidak's test;  
394 NRP1: P < 0.0001, ACE2: P = 0.374.

395 The bars, error bars and circles represent the mean, SEM and individual data points,  
396 respectively. \*P< 0.05, \*\*P< 0.01, \*\*\*P< 0.001, \*\*\*\*P< 0.0001.

397  
398

399 Fig. S2.

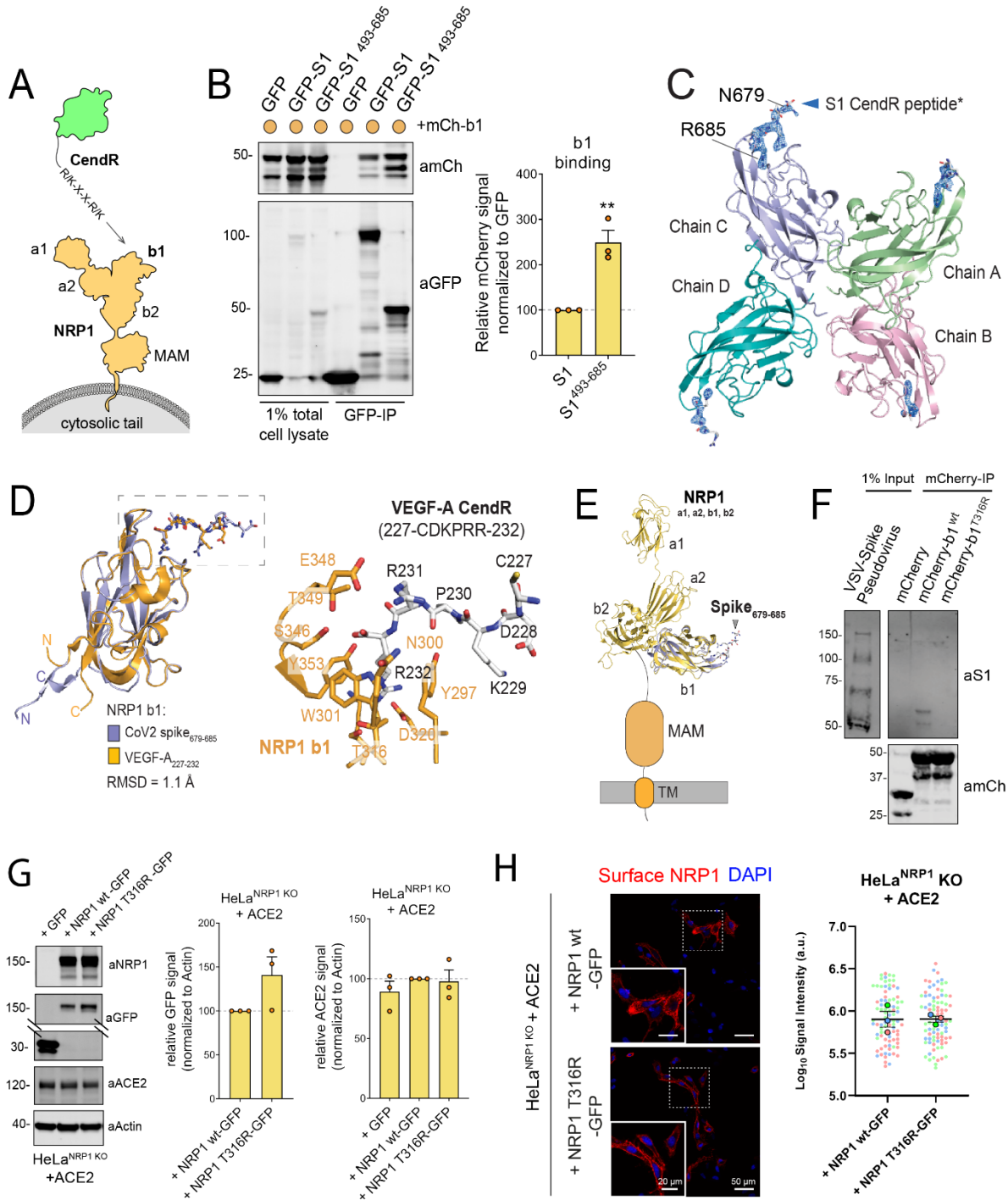


400  
401

402 **Fig. S2. Image processing and phenotyping of SARS-CoV-2 infected cells.** (A) Caco-  
403 2 shSCR and shNRP1 cells were infected with VSV pseudotyped with VSV-G for 16 hours, fixed,  
404 and detected by GFP reporter expression (N=3). Two-tailed unpaired t-test. P=0.3187. Scale bar =  
405 500  $\mu\text{m}$ . (B) Schematic of the two-step staining procedure used to distinguish external from  
406 internal virus particles. (C) Original image of SARS-CoV-2 N signal (green) and enhanced image  
407 (red) using UNET deep learning algorithm. (D) Single-cell segmentation of the nuclei  
408 using the nucleAIzer deep learning algorithm, and the cytoplasmic region based on  
409 global thresholding of the UNET enhanced image. (E) Morphology, shape and intensity features  
410 of single-cells and their microenvironment are extracted. Features include morphology, intensity  
411 and texture descriptor numbers.  $C_i$ : features of the i-th cell,  $C_j$ : features of the j-th cell. (F)  
412 Machine learning-based phenotyping of single cells into non-infected, single-nuclei infected and  
413 multinucleated cells. (G) Ratio of syncytia and single cell infection phenotypes in HeLa<sup>wt</sup>+ACE2  
414 and HeLa<sup>NRP1 KO</sup>+ACE2 cells infected with SARS-CoV-2. Cells were fixed at 16 hpi and stained  
415 for N protein (magenta) and Hoechst (cyan), and cell phenotypes were quantified (N=3). Scale bar  
416 = 20  $\mu\text{m}$ . (H) HeLa<sup>wt</sup>+ACE2 and HeLa<sup>NRP1 KO</sup>+ACE2 cells were infected with SARS-CoV-2  
417  $\Delta\text{S1/S2}$ . Cells were fixed at 6 or 16 hpi and stained as in (G), and virus infectivity was quantified  
418 (N=3). Two-tailed unpaired t-test; P=0.12 and P<0.0001. Scale bar=200  $\mu\text{m}$ . (I) Ratio of syncytia  
419 and single cell infection phenotypes in HeLa<sup>wt</sup>+ACE2 and HeLa<sup>NRP1 KO</sup>+ACE2 cells infected with  
420 SARS-CoV-2  $\Delta\text{S1/S2}$ . Cells were fixed and stained as in (G). Scale bar = 20  $\mu\text{m}$ .  
421 The bars, error bars, circles and triangles represent the mean, SD and individual data points,  
422 respectively. \*P< 0.05, \*\*P< 0.01, \*\*\*P< 0.001, \*\*\*\*P< 0.0001.

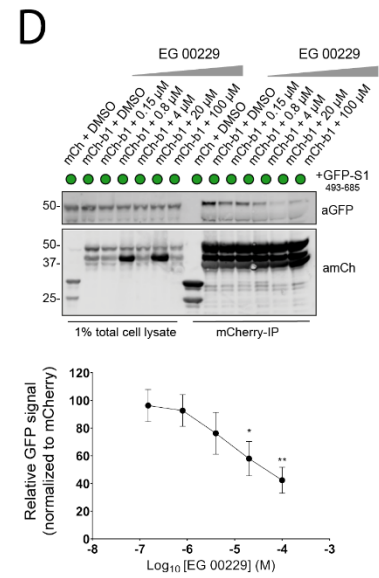
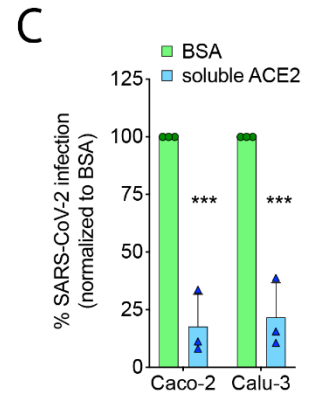
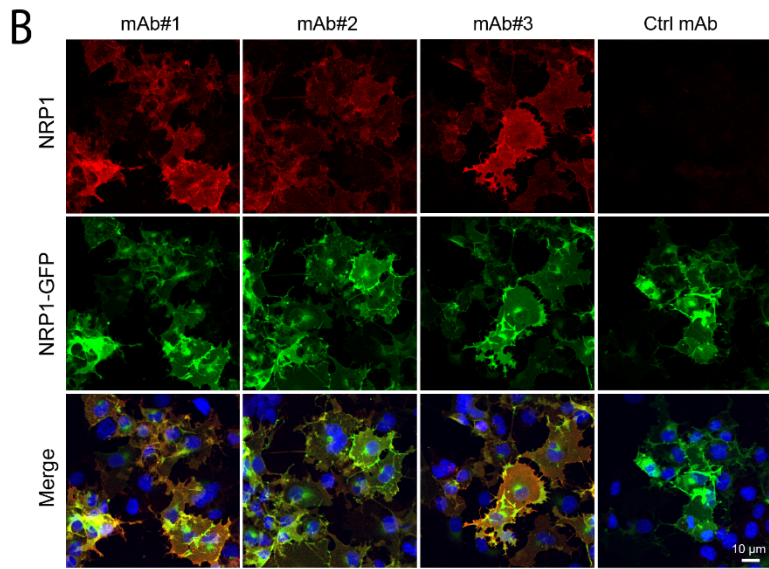
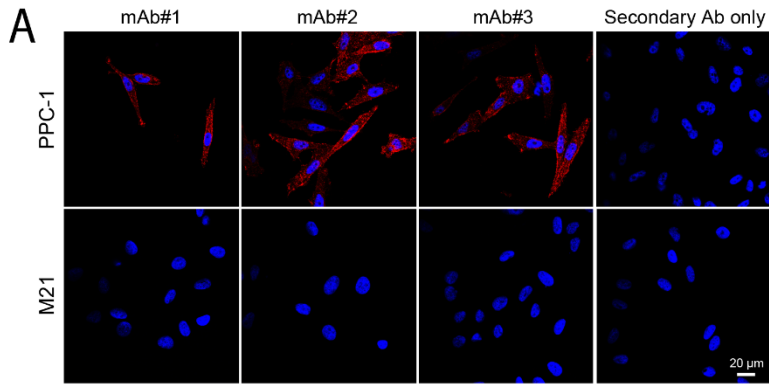
423

424 **Fig. S3.**  
425



426

427 **Fig. S3. Extended molecular insights into the S1-NRP1 interaction** (A) Schematic of  
428 CendR motif binding to the NRP1 b1 domain. (B) HEK293T cells were co-transfected with  
429 combinations of mCherry-b1, and GFP, GFP-tagged S1 or S1<sup>493-685</sup> and subjected to GFP-nanotrap  
430 (N=3). Two-tailed unpaired t-test; P = 0.0050. (C) Ribbon representation of NRP1 b1 –  
431 S1 CendR peptide complex. The electron density shown corresponds to a simulated-annealing  
432 OMIT Fo – Fc map of S1 CendR peptide contoured at 3 $\sigma$ . For clarity, the S1 CendR peptide binds  
433 to chain C of NRP1 B1 domain showing the electron density from N679 to R685 was selected for  
434 structural analysis and figure display. (D) Left: NRP1 b1 – S1 CendR peptide complex superposed  
435 with NRP1 b1 – VEGF-A fusion complex (PDB ID: 4DEQ). Right: enlarged view highlighting  
436 the binding of VEGF-A<sub>227-232</sub> to NRP1 b1. Bound peptides and key binding residues on b1 are shown  
437 in stick representation. (E) NRP1 b1 – S1 CendR peptide complex superposed with NRP1  
438 a1a2b1b2 structure (PDB ID: 4GZ9). (F) HEK293T cells were co-transfected with mCherry,  
439 mCherry-NRP1 b1 or mCherry-NRP1 b1 T316R and the mCherry-tagged proteins were captured  
440 on mCherry-beads. VSV-S pseudoparticles were then added and subjected mCherry-  
441 nanotrap (N=3). (G) HeLa<sup>NRP1 KO</sup>+ACE2 cells were transfected with GFP, NRP1 wt-GFP or NRP1  
442 T316R-GFP and lysed 24 h later (N=3). GFP levels: Two-tailed unpaired t-test, P = 0.1167. ACE2  
443 levels: one-way ANOVA and Dunnett's test; +NRP1 wt-GFP vs + GFP, P = 0.5293; +NRP1 wt-  
444 GFP vs + NRP1 T316R-GFP, P = 0.9672. (H) IF staining of HeLa<sup>NRP1 KO</sup>+ ACE2 transfected with  
445 NRP1 wt-GFP and NRP1 T316R-GFP. Non-permeabilised cells were labelled with anti-NRP1  
446 mAb#3, and signal intensity was quantified using Volocity software (N=3, 88 cells per  
447 condition). Two-tailed unpaired t-test; P = 0.9829. Scale bar = 50  $\mu$ m and 20  $\mu$ m (zoom panel).  
448 The bars, error bars and circles represent the mean, SEM and individual data points,  
449 respectively. \*P< 0.05, \*\*P< 0.01, \*\*\*P< 0.001, \*\*\*\*P< 0.0001.



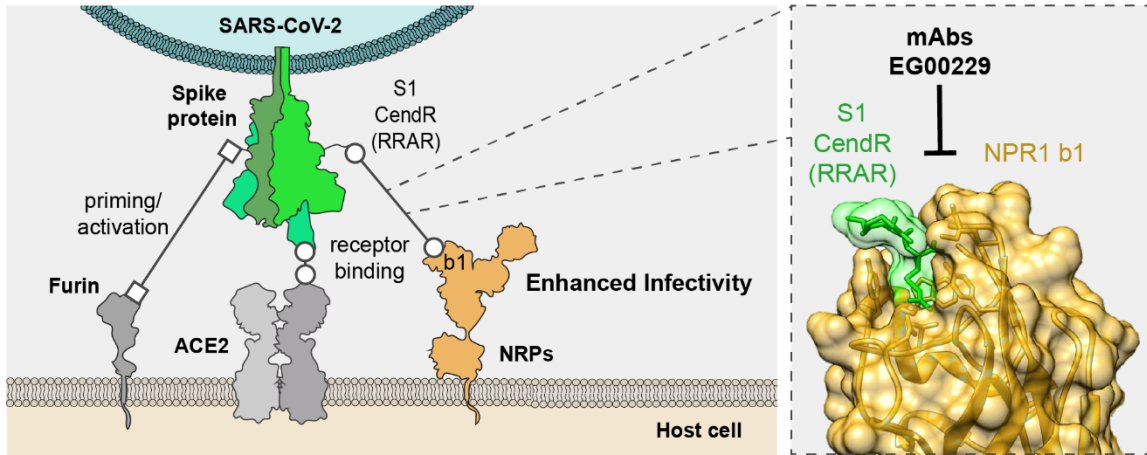
452 **Fig. S4. Validation of selective inhibitors for SARS-CoV-2 infection.** (A) Fluorescence  
453 confocal images of non-permeabilised NRP1-positive PPC-1 and NRP1-negative M21 cells  
454 incubated with mAb#1, #2 and #3 (N=2). Antibody staining (red) and DAPI (blue) are  
455 shown. Scale bar=20  $\mu\text{m}$ . (B) Fluorescent spinning-disk confocal images of Cos7 cells expressing  
456 human NRP1-GFP using mAb#1, #2, #3 and ctrl mAb against influenza HA. Non-permeabilised,  
457 fixed cells in 96-well plates were incubated with the mAbs (1:10 dilution) for 1 h and  
458 immunostained with the secondary antibody AlexaFluor 594 goat anti-mouse IgG. Z- stack images  
459 were acquired using a 20x objective and maximum projections are shown (N=3). Blue: Hoechst;  
460 Green: GFP; Red: antibody signal. Scale bar=10  $\mu\text{m}$ . (C) Inhibition of SARS-CoV-2 infection by  
461 treatment with recombinant soluble ACE2 in Caco-2 and Calu-3 cells. Cells were pre-treated  
462 with soluble ACE2 (10  $\mu\text{g}/\text{mL}$ ) for 1 h prior to SARS-CoV-2 infection. At 16 hpi the cells were  
463 fixed and stained for N protein and infection was quantified (N=3). Two-tailed unpaired t-test;  
464  $P=0.0005$  and  $0.0008$ . (D) EG00229 inhibits GFP-S1<sup>493-685</sup> immunoprecipitation. HEK293T cells  
465 were co-transfected with GFP-tagged S1<sup>493-685</sup> and mCherry or mCherry-b1, and subjected to  
466 a mCherry-nanotrap in the presence of the indicated concentrations of EG00229 or DMSO  
467 (N=6). Ordinary one-way ANOVA with Dunnett's multiple comparisons test,  $P = 0.9996$  (0.15  
468  $\mu\text{M}$ ),  $0.9866$  (0.8  $\mu\text{M}$ ),  $0.4265$  (4  $\mu\text{M}$ ),  $0.0473$  (20  $\mu\text{M}$ ) and  $0.0041$  (100  $\mu\text{M}$ ). The bars, error bars,  
469 circles and triangles represent the mean, SD (C) and SEM (D) respectively.

470 \* $P < 0.05$ , \*\* $P < 0.01$ , \*\*\* $P < 0.001$ , \*\*\*\* $P < 0.0001$ .

471



472 **Fig S5.**



473

474 **Fig. S5. Model of neuropilin binding in SARS-CoV-2 infection.** The S1 protein of SARS-CoV-  
475 2 associates to neuropilins through CendR peptide recognition by the neuropilin b1 domain. This  
476 interaction promotes SARS-CoV-2 entry and infection in physiologically relevant cell lines. The  
477 ability to target this specific interaction may provide a route for COVID-19 therapies.  
478

479 **Table S1. Thermodynamic parameters for the binding of NRP1 B1 domain with S1 CendR**  
 480 **peptide**

	$K_d$	$\Delta H$	$\Delta G$	$-T\Delta S$	$N^c$
	( $\mu\text{M}$ )	(kcal/mol)	(kcal/mol)	(kcal/mol)	
<b>S1 CendR peptide (pH 7.5)<sup>a</sup></b>					
Native	$20.3 \pm 2.0$	$-3.4 \pm 0.8$	$-6.5 \pm 0.06$	$-3.1 \pm 0.8$	1
R685A	No binding detected				
<b>S1 CendR peptide (pH 5.5)<sup>b</sup></b>					
Native	$13.0 \pm 1.3$	$-7.4 \pm 0.6$	$-6.8 \pm 0.06$	$0.6 \pm 0.7$	1
R685A	No binding detected				

481 a. Experiment performed in buffer containing 50 mM Tris-HCl pH 7.5, 150 mM NaCl.

482 b. Experiment performed in buffer containing 50 mM Sodium citrate pH 5.5, 150 mM  
 483 NaCl.

484 c. Stoichiometry was refined and fixed as 1.0 for calculation.

485

486 **Table S2. Thermodynamic parameters for the binding of NRP1 B1 domain with EG00229**  
 487 **inhibitor in the presence of S1 CendR peptide**

	$K_d$	$\Delta H$	$\Delta G$	$-T\Delta S$	$N^c$
	( $\mu\text{M}$ )	(kcal/mol)	(kcal/mol)	(kcal/mol)	
<b>Titrating EG00229 into NRP1 B1</b>					
pH 7.5 <sup>a</sup>	5.1 ± 0.3	-10.7 ± 0.5	-7.4 ± 0.04	3.3 ± 0.5	1.0
pH 5.5 <sup>b</sup>	9.7 ± 0.2	-11.8 ± 0.6	-7.0 ± 0.01	4.8 ± 0.6	1.0
<b>Titrating EG00229 into NRP1 B1 + S1 CendR peptide</b>					
pH 7.5 <sup>a</sup>	6.3 ± 0.7	-4.5 ± 0.3	-7.2 ± 0.07	-2.7 ± 0.2	1.0
pH 5.5 <sup>b</sup>	14.7 ± 1.5	-2.2 ± 0.1	-6.7 ± 0.06	-4.5 ± 0.2	1.0
<b>Titrating S1 CendR peptide into NRP1 B1 + EG00229</b>					
In pH 7.5 condition	>300	-4.1 ± 1.6	-4.8 ± 0.07	-0.7 ± 1.8	1.0
In pH 5.5 condition	>300	-5.7 ± 0.5	-4.8 ± 0.04	0.9 ± 0.5	1.0

488 a. Experiment performed in buffer containing 50 mM Tris-HCl pH 7.5, 150 mM NaCl.

489 b. Experiment performed in buffer containing 50 mM Sodium citrate pH 5.5, 150 mM  
 490 NaCl.

491 c. Stoichiometry was refined and fixed as 1.0 for calculation.

492

493 **Table S3. Summary of crystallographic structure determination statistics**

<b>Data collection statistics</b>	<b>7JJC</b>
Space group	P2 <sub>1</sub> 2 <sub>1</sub> 2 <sub>1</sub>
Resolution (Å)	46.39 – 2.36 (2.45 – 2.36)
a, b, c (Å)	89.93, 89.89, 108.30
α, β, γ (°)	90, 90, 90
Total observations	276,344 (27,837)
Unique reflections	36,732 (3,656)
Completeness (%)	99.6 (96.2)
R <sub>merge</sub> <sup>+</sup>	0.100 (1.478)
R <sub>pim</sub> *	0.039 (0.565)
CC1/2	0.999 (0.613)
<I/σ(I)>	11.4 (1.0)
Multiplicity	7.5 (7.6)
Molecule/asym.	4
<b>Refinement statistics</b>	
R <sub>work</sub> /R <sub>free</sub> (%) <sup>§#</sup>	20.2/24.9
No. protein atoms, Ligand (peptide), Waters	5217, 128, 144
Wilson B (Å <sup>2</sup> )	50.6
Average B (Å <sup>2</sup> ) <sup>^</sup>	54
Protein (chain A/B/C/D)	52/53/51/55
S1 CendR peptide (chain E/F/G/H)	79/81/87/90
Water	51
rmsd bonds (Å), angles (°)	0.003, 0.687
Ramachandran plot: Favored/outliers (%)	95.7/1.1

494 Values in parentheses refer to the highest resolution shell.  $*R_{\text{merge}} = \sum |I - \langle I \rangle| / \sum \langle I \rangle$ , where  $I$  is the intensity of each individual reflection.  $*R_{\text{pim}}$   
495 indicates all  $I^+$  &  $I^-$ .  $*R_{\text{work}} = \sum |F_o - F_c| / \sum |F_o|$ , where  $F_o$  and  $F_c$  are the observed and calculated structure-factor amplitudes for each reflection  $h$ .  
496  $*R_{\text{free}}$  was calculated with 10% of the diffraction data selected randomly and excluded from refinement.  $^{\wedge}$ Calculated using Baverage.  
497  
498